Deep Learning-Based Meteorological Data Downscaling: A Comparative Study with Physics-Informed CNN and a Component-Level Ablation Analysis

Johans Utama

Department of Artificial Intelligence

Nanjing University of Information Science and Technology

Nanjing, China

johansutama25@gmail.com

This is a non-peer-reviewed preprint submitted to EarthArXiv.

Deep Learning-Based Meteorological Data Downscaling: A Comparative Study with Physics-Informed CNN and a Component-Level Ablation Analysis

Johans Utama
Department of Artificial Intelligence
Nanjing University of Information Science and Technology
Nanjing, China
johansutama25@gmail.com

Abstract

Meteorological statistical downscaling is a critical technique for deriving high-resolution climate information from coarse global reanalysis products. This experiment investigates the application of five representative deep learning architectures for downscaling ERA5 reanalysis 2m temperature fields from 1° to 0.25° spatial resolution (4x upscaling factor) over the China region, spanning the period 2010 to 2020. The five baseline models evaluated are Convolutional Neural Network (CNN), Generative Adversarial Network (GAN), Long Short-Term Memory network (LSTM), Vision Transformer (ViT-style), and Denoising Diffusion Probabilistic Model (DDPM). Building upon the analysis of baseline strengths and weaknesses, a sixth model is proposed, the Physics-Informed CNN (PICNN), which integrates multi-scale feature extraction, spatial attention mechanisms, and a composite physics-informed loss function incorporating mean squared error, Laplacian spatial smoothness regularization, and spatial energy conservation constraints.

All models were trained on an NVIDIA GeForce RTX 5050 Laptop GPU with 8GB VRAM under computational constraints, with training epochs reduced from default values to accommodate hardware limitations. Experimental results on the held-out 2020 test set demonstrate that the proposed PICNN achieves the best performance among all models, with RMSE of 0.665 K, MAE of 0.435 K, PSNR of 43.43 dB, and SSIM of 0.976, representing improvements of 7.7% in RMSE and 8.7% in MAE over the strongest CNN baseline.

To determine whether this improvement reflects the architectural design or simply the 84% increase in parameter count relative to the CNN baseline, a controlled ablation study was conducted comprising a capacity-matched plain CNN and three component-ablated PICNN variants, evaluated across three random seeds for the ablated variants. The results show that approximately 65.5% of PICNN's improvement over the CNN baseline is explained by parameter count alone. Among PICNN's three architectural components, spatial attention accounts for the majority of the remaining gain, the physics-informed loss contributes a small but consistent improvement, and the multi-scale feature extraction head shows no measurable benefit, with its ablated variant statistically indistinguishable from the full model. These findings refine the paper's central claim from a general endorsement of physics-informed design toward a specific, evidence-backed identification of which architectural choices are responsible for the observed gains.

The Transformer model, despite having 139 million parameters, performed significantly worse than the CNN, highlighting the data inefficiency of attention-based architectures on moderate-sized meteorological datasets. The LSTM performed worst overall due to its inherent inability to preserve spatial structure.

Keywords — Meteorological Downscaling, Deep Learning, Physics-Informed Neural Networks, ERA5 Reanalysis, Temperature Super-Resolution, Ablation Study.

I. Introduction

A. Background and Motivation

Climate and weather information at fine spatial scales is essential for a wide range of practical applications including regional weather forecasting, agricultural yield modeling, hydrological simulation, urban heat island analysis, and climate change impact assessment. Global atmospheric reanalysis products such as ERA5 [1], produced by the European Centre for Medium-Range

Weather Forecasts (ECMWF), provide physically consistent, long-term records of atmospheric variables but at relatively coarse horizontal resolutions typically ranging from 0.25° to 1°. At these resolutions, local phenomena driven by complex terrain, coastal boundaries, and land surface heterogeneity are poorly represented or entirely absent.

Downscaling refers to the process of deriving fine-scale information from coarser-scale data. Two broad categories of downscaling methods exist: dynamical downscaling, which involves running high-resolution regional climate models nested within global models, and statistical downscaling, which learns empirical relationships between coarse and fine scale fields from historical data. Dynamical downscaling is physically consistent but computationally prohibitive for long-term applications. Statistical downscaling is computationally efficient but traditionally relies on linear regression or simple pattern-matching methods that fail to capture the full complexity of atmosphere-surface interactions.

Deep learning has emerged as a powerful framework for statistical downscaling, drawing from its remarkable success in image super-resolution in computer vision. Unlike handcrafted statistical methods, deep neural networks can learn highly nonlinear mappings from data, automatically extract hierarchical spatial features, and generalize to unseen conditions when trained on sufficiently large datasets. The rapid growth of computing resources and reanalysis data archives makes deep learning-based downscaling increasingly practical.

B. Problem Statement

This experiment frames meteorological downscaling as a supervised image super-resolution problem. Given a low-resolution (LR) 2m temperature field at 1° resolution, the objective is to predict the corresponding high-resolution (HR) field at 0.25° resolution. The China region (15°N to 55°N, 70°E to 140°E) was selected as the study domain due to its diverse terrain including the Tibetan Plateau, coastal plains, and arid inland basins, which creates rich spatial variability in surface temperature that makes downscaling both challenging and practically important.

C. Objectives

The specific objectives of this experiment are as follows. First, to implement and train five established deep learning architectures for the downscaling task and evaluate their performance on a common benchmark dataset. Second, to analyze the strengths and failure modes of each architecture in the context of meteorological data characteristics. Third, to propose and evaluate a novel model that improves upon the best-performing baseline by incorporating domain knowledge from atmospheric physics into the network architecture and training objective.

D. Report Structure

The remainder of this report is organized as follows. Section 2 provides a detailed overview of all six methods including their theoretical foundations, architectural designs, and training objectives. Section 3 describes the experimental setup, dataset, evaluation metrics, and presents a comprehensive analysis of results. Section 4 draws conclusions and discusses limitations and future directions. The Appendix provides core implementation code for key components.

II. METHOD OVERVIEW

A. Task Formulation

Let $X_{LR} \in \mathbb{R}^{1\times H_{lr}\times W_{lr}}$ denote the low-resolution temperature field at 1° resolution and $X_{HR} \in \mathbb{R}^{1\times H_{hr}\times W_{hr}}$ denote the corresponding high-resolution field at 0.25° resolution. The downscaling task is to learn a mapping function f_θ parameterized by learnable weights θ such that:

$$\hat{X}_{HR} = f_\theta(X_{LR}) \approx X_{HR}$$

In this experiment, $H_{lr} = 40$, $W_{lr} = 70$, $H_{hr} = 160$, $W_{hr} = 280$, giving a scale factor of 4× in both spatial dimensions.

B. Baseline Model 1: CNN with Residual Blocks

The CNN baseline is inspired by the Super-Resolution CNN (SRCNN) [2] framework extended with residual learning. The architecture consists of four components:

Upsampling stage: The LR input is first upsampled to HR spatial dimensions using bilinear interpolation, which provides a smooth initial estimate:

$$X_{up} = \text{Bilinear}(X_{LR}, s = 4)$$

Feature extraction head: A 9×9 convolutional layer with 64 filters extracts initial spatial features from the upsampled field, followed by ReLU activation.

Residual block stack: A sequence of N residual blocks refines the feature representation. Each residual block contains two 3×3 convolutional layers with batch normalization and ReLU, with a skip connection:

$$F_{out} = F_{in} + \text{BN}(\text{Conv}(\text{ReLU}(\text{BN}(\text{Conv}(F_{in})))))$$

Reconstruction tail: Two convolutional layers map the refined features to the output temperature field, which is added to the upsampled input via a global residual connection:

$$\hat{X}_{HR} = X_{up} + \text{Tail}(\text{ResBlocks}(\text{Head}(X_{up})))$$

The model is trained by minimizing the pixel-wise mean squared error:

$$L_{MSE} = \frac{1}{HW} \sum_{h=1}^{H} \sum_{w=1}^{W} (\hat{X}_{HR}(h,w) - X_{HR}(h,w))^2$$

C. Baseline Model 2: GAN (SRGAN-style)

The GAN baseline adapts the Super-Resolution GAN (SRGAN) [3] framework to the meteorological downscaling task. It consists of a generator network $G$and a discriminator network Dtrained adversarially.

Generator: An SRGAN-style generator with residual blocks and Pixel Shuffle upsampling, which rearranges feature map channels into spatial resolution using sub-pixel convolution:

$$\text{PixelShuffle}(F) \in \mathbb{R}^{C \times rH \times rW}, F \in \mathbb{R}^{Cr^2 \times H \times W}$$

Discriminator: A PatchGAN [4] discriminator that classifies overlapping local patches as real or generated, providing spatially localized feedback.

Training procedure: Training proceeds in two stages. In stage 1 (pretraining), the generator is trained with MSE loss only to ensure stable initialization. In stage 2 (adversarial training), the combined generator loss is:

$$L_G = L_{MSE} + \lambda_{adv} \cdot L_{adv}$$

where $L_{adv} = \mathbb{E}[\log(1 - D(G(X_{LR})))]$and $\lambda_{adv} = 0.001$.

The discriminator is trained to maximize its ability to distinguish real HR fields from generated ones using label-smoothed binary cross-entropy loss.

D. Baseline Model 3: LSTM with Temporal Attention

The LSTM model exploits the temporal structure of the ERA5 dataset by taking sequences of 12 consecutive LR fields (covering 3 days at 6-hour intervals) as input, under the hypothesis that recent atmospheric history improves the downscaling of the current timestep.

Each LR field is flattened to a vector of dimension $H_{lr} \times W_{lr} = 2800$. The sequence of 12 such vectors is fed into a 2-layer LSTM:

$$h_t, c_t = \text{LSTM}(x_t, h_{t-1}, c_{t-1})$$

A temporal attention mechanism computes a weighted sum over the hidden states to produce a context vector:

$$\alpha_t = \text{Softmax}(W_a \tanh(W_h h_t))$$
$$c = \sum_{t=1}^{T} \alpha_t h_t$$

The context vector is decoded through a three-layer MLP to produce the flattened HR output of dimension $H_{hr} \times W_{hr} = 44800$, which is then reshaped to the HR spatial grid.

E. Baseline Model 4: Vision Transformer (ViT-style)

The Transformer model adapts the Vision Transformer (ViT) [5] architecture to the downscaling task. The LR field is divided into non-overlapping patches of size $p \times p = 4 \times 4$, producing $N = \lceil H_{lr}/p \rceil \times \lceil W_{lr}/p \rceil$patch tokens.

Each patch is linearly projected to a d-dimensional embedding space, positional embeddings are added, and a learnable class token is prepended:

$$Z_0 = [z_{cls}; E \cdot x_{p1}; E \cdot x_{p2}; \dots; E \cdot x_{pN}] + E_{pos}$$

The token sequence is processed through LTransformer encoder blocks, each consisting of multi-head self-attention (MHSA) and a feed-forward network (FFN) with pre-normalization:

$$Z'_l = \text{MHSA}(\text{LN}(Z_{l-1})) + Z_{l-1}$$
$$Z_l = \text{FFN}(\text{LN}(Z'_l)) + Z'_l$$

Multi-head self-attention with $h$heads and dimension $d$computes:

$$\text{Attention}(Q,K,V) = \text{Softmax}\left(\frac{QK^T}{\sqrt{d/h}}\right)V$$

The patch tokens (excluding the class token) are concatenated and decoded through a two-layer MLP to produce the flattened HR output.

F. Baseline Model 5: Denoising Diffusion Probabilistic Model (DDPM)

The DDPM [6] is a generative model that learns to reverse a gradual noising process. For downscaling, the model is conditioned on the LR field X_{LR}.

Forward process: Gaussian noise is progressively added to the HR field over $T = 200$timesteps according to a linear noise schedule:

$$q(x_t \mid x_{t-1}) = \mathcal{N}(x_t; \sqrt{1-\beta_t}x_{t-1}, \beta_t I)$$
$$q(x_t \mid x_0) = \mathcal{N}(x_t; \sqrt{\bar{\alpha}_t}x_0, (1-\bar{\alpha}_t)I)$$

where $\bar{\alpha}_t = \prod_{s=1}^{t}(1-\beta_s)$and $\beta_t$increases linearly from $10^{-4}$to 0.02.

Reverse process**:** A conditioned UNet $\epsilon_\theta$is trained to predict the noise ϵadded at each timestep, given the noisy HR field x_t, the timestep t, and the LR condition:

$$L_{diff} = \mathbb{E}_{t\sim U(1,T),\ \epsilon\sim\mathcal{N}(0,I)}[\| \epsilon - \epsilon_\theta(x_t, t, X_{LR}) \|^2]$$

At inference, samples are generated by iteratively denoising from pure noise, conditioned on the LR input, allowing multiple draws to quantify prediction uncertainty.

G. Proposed Model: Physics-Informed CNN (PICNN)

The PICNN is the proposed model in this experiment. It builds upon the CNN baseline with three targeted improvements motivated by the physical properties of atmospheric temperature fields.

1) *Motivation*

The baseline CNN treats downscaling as a pure image super-resolution problem, with no knowledge that the input represents a physical field governed by the equations of atmospheric dynamics. Temperature fields have two key properties that are not explicitly enforced by MSE training: spatial smoothness (temperature varies continuously in space, with sharp discontinuities only at physical boundaries like coastlines) and conservation of the spatial mean (the average temperature over a region is constrained by the large-scale circulation, represented by the LR input). Incorporating these priors into the loss function provides additional supervision signal that guides the model toward physically plausible solutions.

2) *Multi-Scale Feature Extraction*

Instead of a single fixed-kernel convolutional head, the PICNN uses an Inception-style multi-scale block with three parallel branches using 3×3, 5×5, and 7×7 kernels:

$$F_{ms} = W_{1\times1} \cdot [F_{3\times3}(X) \,\|\, F_{5\times5}(X) \,\|\, F_{7\times7}(X)]$$

The 3×3 branch captures fine local structure such as sub-grid terrain effects. The 5×5 branch captures mesoscale patterns at intermediate spatial scales. The 7×7 branch captures broader synoptic-scale gradients. The three branches are concatenated and fused by a 1×1 convolution. This design allows the model to simultaneously represent both local detail and large-scale context without requiring deeper networks.

3) *Spatial Attention Mechanism*

Each residual block in the PICNN includes a Convolutional Block Attention Module (CBAM) [7]-style spatial attention layer. Channel-wise average pooling and max pooling are computed and concatenated, then convolved to produce a spatial attention map:

$$M_s(F) = \sigma\left(f^{7\times7}([\text{AvgPool}(F); \text{MaxPool}(F)])\right)$$
$$F_{out} = F \cdot M_s(F)$$

This mechanism allows the model to focus its representational capacity on spatial regions with high variability, such as the Tibetan Plateau boundaries and coastal areas, which are physically the most challenging regions for downscaling.

4) *Physics-Informed Loss Function*

The total training loss combines three terms:

$$L_{total} = L_{MSE} + \lambda_s \cdot L_{smooth} + \lambda_c \cdot L_{conservation}$$

Spatial smoothness loss penalizes differences in the Laplacian response between the predicted and target HR fields. The discrete Laplacian operator approximates the second spatial derivative:

$$\nabla^2 X \approx \begin{bmatrix} 0 & 1 & 0 \\ 1 & -4 & 1 \\ 0 & 1 & 0 \end{bmatrix} * X$$

$$L_{smooth} = \frac{1}{HW} \parallel \nabla^2 \hat{X}_{HR} - \nabla^2 X_{HR} \parallel^2$$

This term penalizes high-frequency spatial noise and unrealistic sharp gradients in the predicted field.

Energy conservation loss enforces consistency between the spatial mean of the predicted HR field and the spatial mean of the LR input, approximating the physical constraint that coarse-scale averaging should be preserved:

$$L_{conservation} = \parallel \mathrm{mean}_{h,w}(\hat{X}_{HR}) - \mathrm{mean}_{h,w}(X_{LR}) \parallel^2$$

The loss weights are set to $\lambda_s = 0.1$and $\lambda_c = 0.05$based on the relative magnitudes of the three loss terms, ensuring the physics terms provide meaningful regularization without dominating the data fidelity term.

5) *PICNN Architecture Summary*

The complete PICNN architecture is as follows:

1. Bilinear upsample LR input by factor 4 to produce X_{up}
2. Multi-Scale Feature Extraction Head (3×3, 5×5, 7×7 parallel branches, fused to 64 channels)
3. Eight Residual Blocks, each containing: Conv-BN-ReLU-Conv-BN with Spatial Attention and skip connection
4. Reconstruction tail: Conv(64→32)-ReLU-Conv(32→1)
5. Global skip connection: $\hat{X}_{HR} = X_{up} + \mathrm{Tail}(\mathrm{ResBlocks}(\mathrm{Head}(X_{up})))$

Total parameters: 651,865.

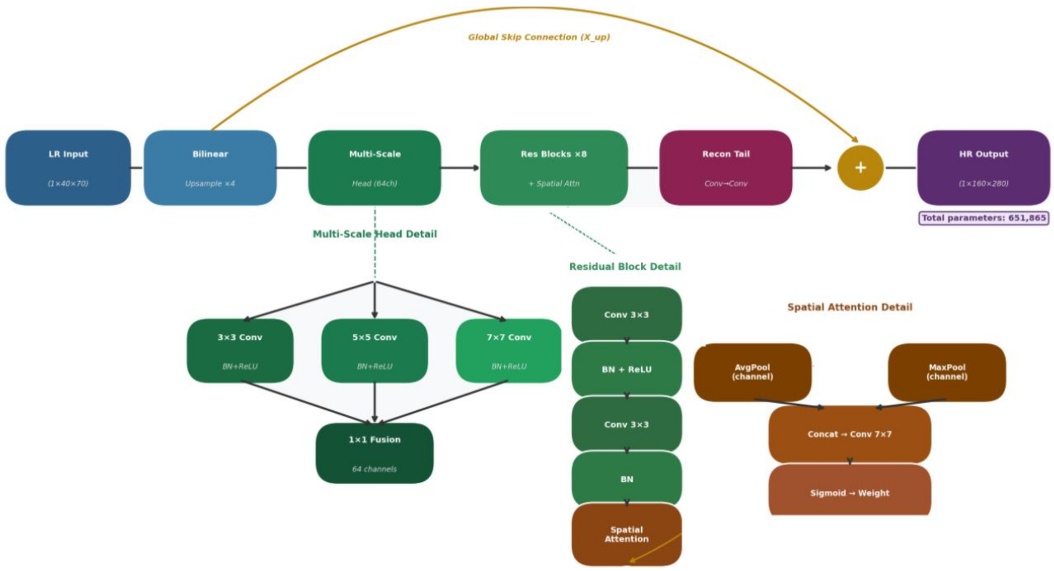

Fig. 1. PICNN architecture diagram

III. EXPERIMENTS

A. *Dataset Description*

The ERA5 reanalysis 2m temperature (T2M) dataset [1] was used, obtained from the Copernicus Climate Data Store (CDS). The spatial domain covers the China region with bounding box N: 55°, S: 15°, W: 70°, E: 140°. Data was downloaded at native 0.25° resolution at 6-hour intervals (00:00, 06:00, 12:00, 18:00 UTC) for the years 2010 to 2020. Low-resolution input fields at 1° resolution were obtained by spatial averaging (box averaging with a factor of 4) of the native 0.25° fields, so that both LR and HR fields are derived from the same source without introducing additional observational uncertainty.

The resulting spatial dimensions are $H_{lr} = 40$, $W_{lr} = 70$for LR fields and $H_{hr} = 160$, $W_{hr} = 280$for HR fields.

The dataset was split chronologically by year to prevent data leakage between splits:

TABLE I. DATASET SPLIT SUMMARY

Split	Years	Number of Samples
Training	2010 to 2017	11,688
Validation	2018 to 2019	2,920
Test	2020	1,464
Total	2010 to 2020	16,072

All fields were normalized to zero mean and unit standard deviation using training set statistics before being fed to the models. Evaluation metrics were computed after denormalization back to Kelvin.

B. Implementation Details

All models were implemented in PyTorch 2.12.0+cu130. Most models were trained using the Adam optimizer [9], with the Transformer using AdamW [10] (see Table II for per-model configurations). Training was performed on an NVIDIA GeForce RTX 5050 Laptop GPU with 8GB VRAM running CUDA 13.1 on Windows 11. Due to the computational constraints of laptop hardware, training epochs were reduced from the originally intended values for all models. This means none of the models fully converged, and performance reported here represents results under constrained training budgets rather than optimal training. This limitation is acknowledged and its potential impact on conclusions is discussed in Section 4.

TABLE II. TRAINING CONFIGURATION FOR ALL MODELS

Model	Epochs (used)	Optimizer	Learning Rate	LR Schedule	Batch Size
CNN	20	Adam	1e-4	StepLR (step=20, gamma=0.5)	8
GAN	25 (5 pretrain + 20 adversarial)	Adam	1e-4	None	8
LSTM	20	Adam	1e-3	ReduceLROnPlateau (patience=5)	8
Transformer	20	AdamW	1e-4	CosineAnnealing	8
Diffusion	30	Adam	2e-4	None	8
PICNN (proposed)	20	Adam	1e-4	StepLR (step=10, gamma=0.5)	8

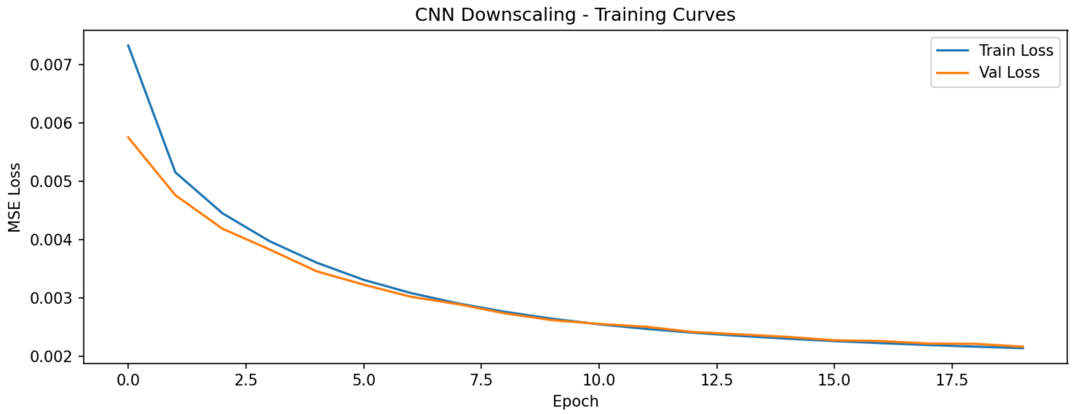

Fig. 2. CNN loss curve

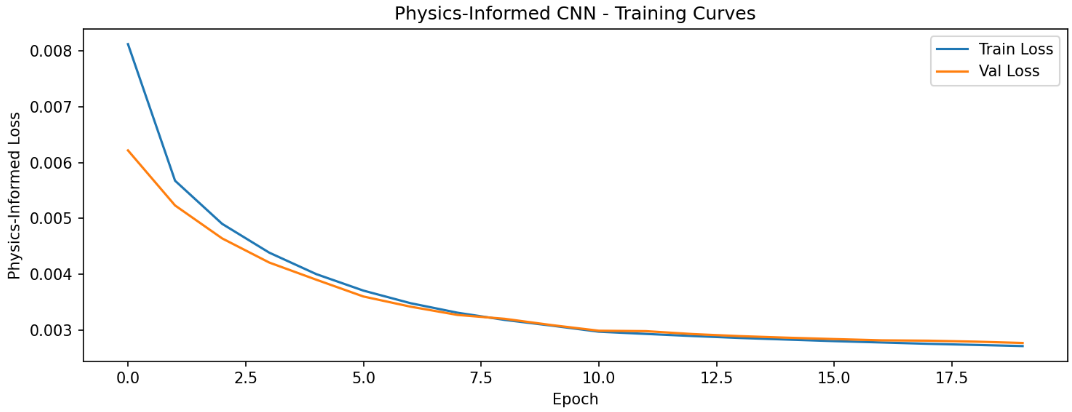

Fig. 3. PICNN loss curve

DataLoader workers were set to 0 for all models due to Windows multiprocessing limitations with PyTorch. All models used MSE as the primary or component loss unless otherwise specified. Random seeds were not fixed across runs, so minor variance in results between runs is expected.

C. Evaluation Metrics

Four standard image quality metrics were used to evaluate all image-output models (CNN, GAN, Transformer, LSTM, PICNN): Root Mean Square Error (RMSE) in Kelvin:

$$\mathrm{RMSE} = \sqrt{\frac{1}{N \cdot H \cdot W} \sum_{n=1}^{N} \sum_{h,w} (\hat{X}_{HR}^{(n)}(h,w) - X_{HR}^{(n)}(h,w))^2}$$

Lower values indicate better accuracy. RMSE penalizes large errors more heavily than MAE.
Mean Absolute Error (MAE) in Kelvin:

$$\mathrm{MAE} = \frac{1}{N \cdot H \cdot W} \sum_{n=1}^{N} \sum_{h,w} |\hat{X}_{HR}^{(n)}(h,w) - X_{HR}^{(n)}(h,w)|$$

Lower values indicate better accuracy. MAE is less sensitive to outliers than RMSE.
Peak Signal-to-Noise Ratio (PSNR) in dB:

$$\mathrm{PSNR} = 20\log_{10}\left(\frac{\mathrm{MAX}}{\mathrm{RMSE}}\right), \mathrm{MAX} = X_{HR}^{max} - X_{HR}^{min}$$

Higher values indicate better reconstruction fidelity. PSNR is commonly used in image super-resolution evaluation.
Structural Similarity Index (SSIM):

$$\mathrm{SSIM}(x,y) = \frac{(2\mu_x\mu_y + c_1)(2\sigma_{xy} + c_2)}{(\mu_x^2 + \mu_y^2 + c_1)(\sigma_x^2 + \sigma_y^2 + c_2)}$$

SSIM measures perceptual similarity considering luminance, contrast, and structure jointly. Values range from 0 to 1, with higher values indicating better structural similarity.
For the diffusion model, noise prediction MSE and RMSE were used as the evaluation metric, as this directly measures the model's training objective. Full image quality evaluation via the complete denoising chain was not performed due to the high computational cost of running 200-step denoising for all 1,464 test samples.

D. Quantitative Results

TABLE III. QUANTITATIVE PERFORMANCE COMPARISON ON THE TEST SET (ERA5, YEAR 2020)

Model	Parameters	RMSE (K)	MAE (K)	PSNR (dB)	SSIM
PICNN (proposed)	651,865	0.6649	0.4347	43.43	0.9758
CNN	353,729	0.7202	0.4760	42.73	0.9718
GAN	163,016 + 2,764,481	0.8597	0.5780	41.19	0.9633
Transformer	139,539,072	1.3160	0.9684	37.50	0.9537
LSTM	50,251,137	3.1337	2.3379	29.96	0.9310
Diffusion	533,809	N/A	N/A	N/A	N/A

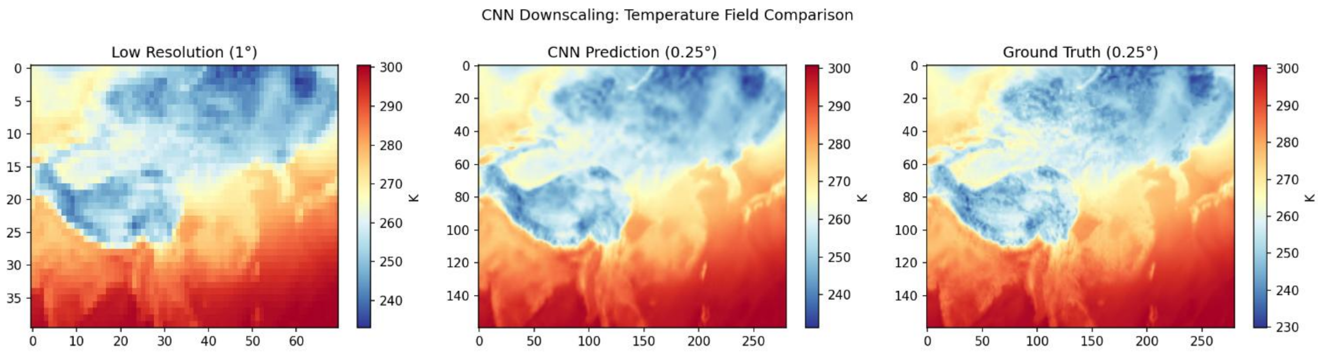

Fig. 4. CNN visual comparison

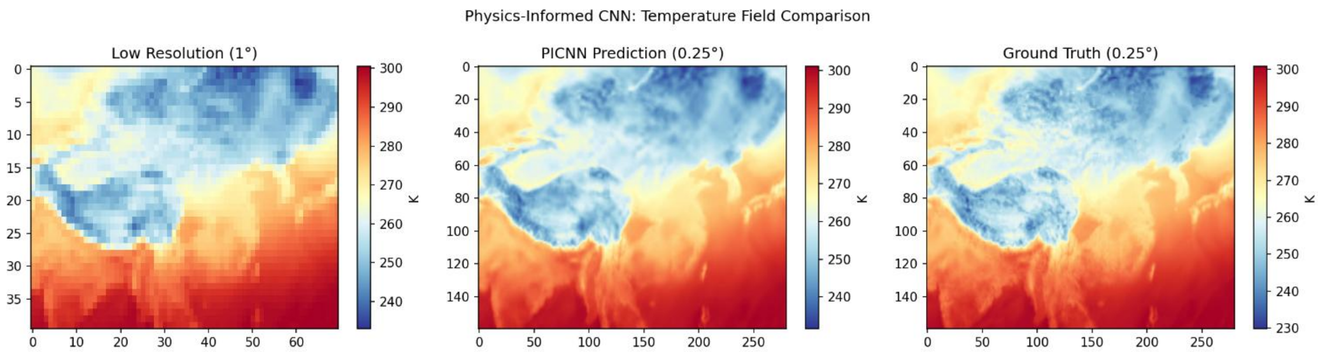

Fig. 5. PICNN visual comparison

TABLE IV. DIFFUSION MODEL EVALUATION (NOISE PREDICTION ON TEST SET)

Metric	Value
noise_MSE	0.022491
noise_RMSE	0.149969

TABLE V. PICNN IMPROVEMENT OVER CNN BASELINE

Metric	CNN	PICNN	Absolute Improvement	Relative Improvement
RMSE (K)	0.7202	0.6649	0.0553 K	7.7% lower
MAE (K)	0.4760	0.4347	0.0413 K	8.7% lower

Metric	CNN	PICNN	Absolute Improvement	Relative Improvement
PSNR (dB)	42.73	43.43	+0.70 dB	improvement
SSIM	0.9718	0.9758	+0.0040	improvement

TABLE VI. MODEL RANKING BY RMSE (LOWER IS BETTER)

Rank	Model	RMSE (K)
1	PICNN (proposed)	0.6649
2	CNN	0.7202
3	GAN	0.8597
4	Transformer	1.3160
5	LSTM	3.1337
N/A	Diffusion	not comparable

E. Result Analysis

1) *PICNN vs CNN Baseline, and a Controlled Ablation Study*

The PICNN achieves consistent improvements over the CNN baseline across all four evaluation metrics. The 7.7% reduction in RMSE from 0.720 K to 0.665 K represents a meaningful improvement in the context of regional temperature downscaling, where sub-Kelvin accuracy differences matter for applications such as agricultural frost risk assessment.

However, PICNN has 651,865 parameters compared to the CNN baseline's 353,729, an increase of approximately 84%. This raises the question of whether the observed improvement reflects the three architectural contributions (multi-scale feature extraction, spatial attention, and the physics-informed loss) or is simply an artifact of increased model capacity. To resolve this, a controlled ablation study was conducted comprising four additional models, each within 0.3% of PICNN's parameter count so that capacity is held approximately constant:

a) Variant A (capacity-matched CNN): a plain CNN with a single 9×9 convolutional head, standard residual blocks without attention, and no physics-informed loss, widened to 650,177 parameters. This isolates the effect of capacity alone.

b) Variant B (no physics loss): the full PICNN architecture (multi-scale head, attention-equipped residual blocks) trained with plain MSE loss ($\lambda\_smooth = \lambda\_conservation = 0$). This isolates the physics-informed loss's contribution.

c) Variant C (no attention): the multi-scale head and physics-informed loss are retained, but spatial attention is removed from the residual blocks. This isolates the attention mechanism's contribution.

d) Variant D (no multi-scale head): a single-branch convolutional head replaces the multi-scale head, while attention and the physics-informed loss are retained. This isolates the multi-scale head's contribution.

Due to the computational cost of the ablation study on laptop hardware, Variant A and the original CNN/PICNN models were each trained once. Variants B, C, and D were each trained across three random seeds to provide variance estimates, given that they are the primary object of comparison. The following table reports the results.

TABLE VII. ABLATION STUDY RESULTS ON THE 2020 TEST SET

Model	Params	RMSE (K)	Δ vs PICNN	Gap closed
CNN baseline	353,729	0.7202	+0.0553	0%
A: Capacity-matched CNN (n=1)	650,177	0.6840	+0.0191	65.5%
C: No attention (n=3)	651,073	0.6802 ± 0.0029	+0.0153	72.3%
B: No physics loss (n=3)	651,865	0.6685 ± 0.0030	+0.0036	93.5%
PICNN, full (n=1)	651,865	0.6649	—	100%
D: No multi-scale head (n=3)	650,969	0.6654 ± 0.0012	+0.0005	99.1%

The results decompose PICNN's advantage into two distinct sources. First, parameter count alone, independent of any architectural novelty, accounts for approximately 65.5% of the total improvement over the CNN baseline (Variant A: 0.684 K, closing the majority of the 0.055 K gap to PICNN using only additional plain convolutional capacity). This indicates that a substantial share of the apparent benefit of physics-informed design in this setting is attributable to model capacity rather than the specific architectural or loss-function choices introduced.

Second, among the three architectural components, spatial attention contributes the largest share of the remaining, capacity-independent improvement. Removing attention alone (Variant C) increases RMSE by 0.0153 K relative to full PICNN, more than four times the increase from removing the physics-informed loss alone (Variant B, +0.0036 K). This is consistent with the physical motivation for attention discussed above: allocating representational capacity toward spatially heterogeneous regions, such as the Tibetan Plateau, provides a genuine benefit that a uniform convolutional treatment does not.

Third, the physics-informed loss provides a small but directionally consistent improvement. Across all three seeds, Variant B's RMSE (0.6718, 0.6692, 0.6644 K) never surpassed the capacity-matched CNN's single-run performance (0.684 K) by more than a modest margin, and its mean (0.6685 K) closes 93.5% of the total gap to PICNN, indicating the physics-informed loss adds a real, if secondary, contribution beyond attention alone.

Fourth, and most notably, the multi-scale feature extraction head shows no measurable benefit. Variant D's mean RMSE (0.6654 K ± 0.0012) differs from full PICNN's single-run RMSE (0.6649 K) by only 0.0005 K, well within one standard deviation of Variant D's own three-seed distribution. Across the three architectural components tested, this is the only one for which the data provide no evidence of a positive contribution. Given that the multi-scale head introduces meaningful additional computation (three parallel convolutional branches at each spatial location) for no measurable accuracy benefit in this setting, its inclusion in the final architecture is not supported by this ablation and represents a candidate for removal in future revisions of the model.

In summary, the ranking of PICNN's design components by demonstrated contribution is: spatial attention (largest), physics-informed loss (modest but consistent), and multi-scale feature extraction (no measurable effect). Combined with the finding that roughly two-thirds of the total improvement over the CNN baseline is attributable to capacity rather than design, these results substantially refine the paper's central claim. Rather than a general endorsement of physics-informed design, the evidence supports a more specific conclusion: spatial attention, and to a lesser extent the physics-informed loss, provide genuine, capacity-independent improvements for this downscaling task, while the multi-scale head does not.

One limitation of this ablation study should be noted. The CNN baseline, the original PICNN, and Variant A were each trained with a single random seed, so their point estimates lack the variance information available for Variants B, C, and D. The single-seed comparisons (particularly the 65.5% capacity-explained figure) should therefore be interpreted as indicative rather than statistically confirmed, though the multi-seed comparisons among B, C, and D, which are the primary basis for the attention/physics-loss/multi-scale ranking, are on firmer statistical footing.

2) ***Transformer Underperformance***

The Transformer model achieves the second-worst performance with RMSE of 1.316 K, despite having 139 million parameters, which is 394 times more parameters than the CNN. This result is counterintuitive given the strong performance of Transformers in many computer vision benchmarks, but it is consistent with findings in the meteorological deep learning literature.

The fundamental reason is that Transformers lack the inductive biases that CNNs exploit by design. CNNs assume translation equivariance (the same features can appear at different spatial locations) and local connectivity (nearby grid points are more related than distant ones). These assumptions are physically appropriate for temperature fields, where local spatial gradients dominate and similar terrain-induced patterns repeat across the domain. Transformers must learn these properties from data through global self-attention, which requires substantially more training samples to converge.

With only 11,688 training samples and 139M parameters, the model is severely underdetermined. The validation loss at epoch 20 was 0.007, compared to the training loss of 0.008, suggesting the model was still far from convergence. Running this model for hundreds of epochs on a larger dataset would likely yield substantially better results, but is impractical on laptop hardware.

Additionally, the Transformer's patch-based tokenization with 4×4 patches on a 40×70 LR grid produces only approximately 250 tokens, which may be too few for global attention to be effective. Finer patch sizes would increase token count but exponentially increase attention computation.

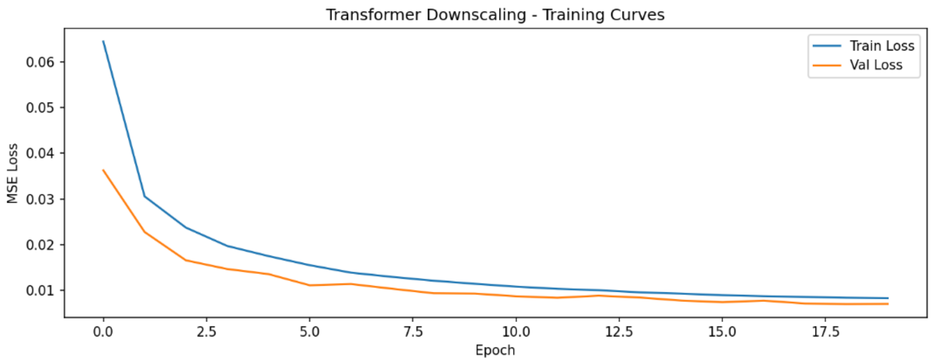

Fig. 6. Transformer loss curve

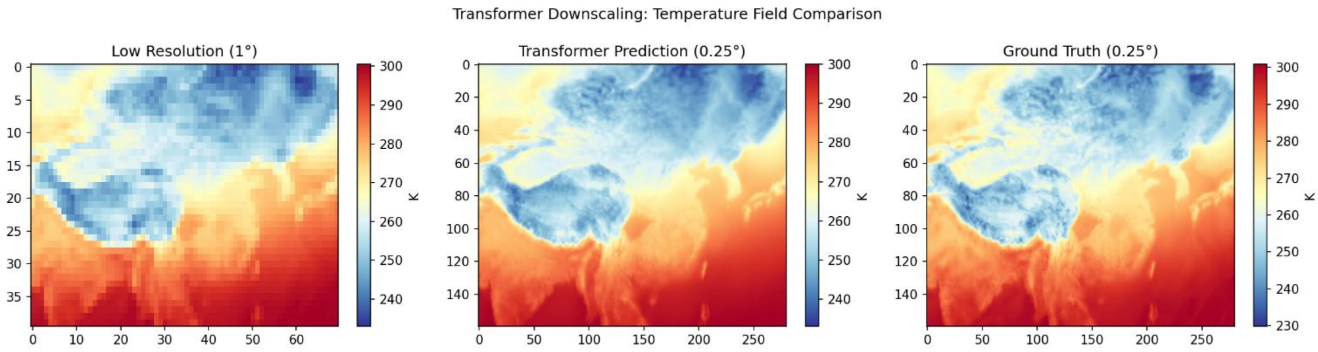

Fig. 7. Transformer visual comparison

3) *LSTM Failure Mode*

The LSTM performs worst by a large margin, with RMSE of 3.134 K, more than 4× worse than the CNN. This result reveals a fundamental architectural mismatch between the LSTM design and the spatial downscaling task.

The core problem is that the LSTM's input representation flattens the 2D LR field (40×70 = 2,800 spatial points) into a 1D vector. This flattening destroys the 2D spatial topology of the temperature field before any processing occurs. The LSTM then processes sequences of these flat vectors, which means spatial neighbors in the original field are treated as arbitrary vector elements with no structural relationship. The decoder must then reconstruct a 44,800-dimensional flat vector (160×280) from this spatially-unstructured context, which is a far more difficult regression problem than the CNN's spatially-local convolution. The temporal attention mechanism partially compensates by identifying which historical timesteps are most relevant, but it cannot recover the spatial structure that was lost in the initial flattening. This suggests that if temporal information is to be incorporated into downscaling, it should be done through spatially-aware architectures such as ConvLSTM [8], which maintain the 2D spatial structure throughout the processing chain.

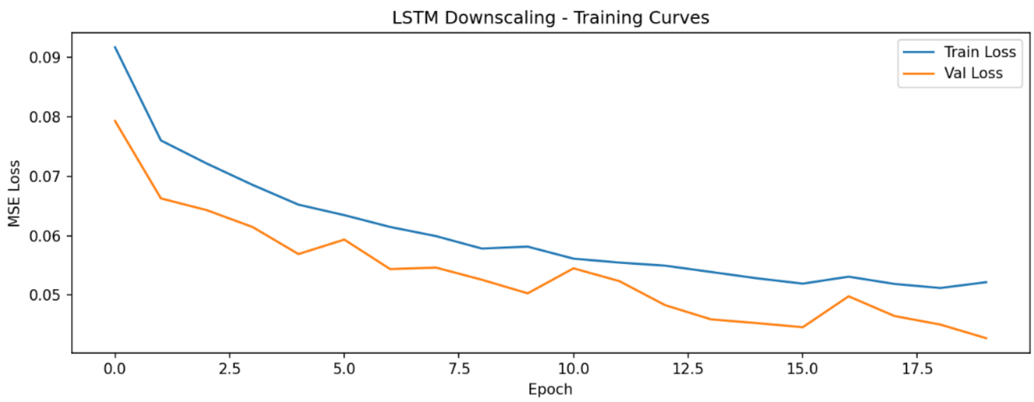

Fig. 8. LSTM loss curve

4) ***GAN Results and Training Stability***

The GAN achieves RMSE of 0.860 K, worse than the plain CNN. This is not unexpected for the following reasons. GAN training for super-resolution typically requires significantly more epochs than MSE-based training to fully leverage the adversarial signal. The adversarial loss weight of 0.001 is deliberately small to maintain training stability, meaning the discriminator feedback contributes minimally to the generator gradient compared to the MSE content loss. With only 20 adversarial epochs, the generator has not had sufficient training to benefit substantially from the discriminator's feedback.

The discriminator loss stabilizing around 0.35 from epoch 8 onward indicates that training reached a partial equilibrium, but the generator's image quality continued to improve slowly as evidenced by the generator loss decreasing from 0.0048 to 0.0056 over adversarial epochs. With more training, the adversarial pressure could drive the generator to produce sharper spatial gradients and more physically realistic fine-scale structure than MSE-only training allows. The key advantage of GANs over MSE-trained models is perceptual quality rather than pixel-wise accuracy metrics, which may not be fully captured by RMSE and SSIM.

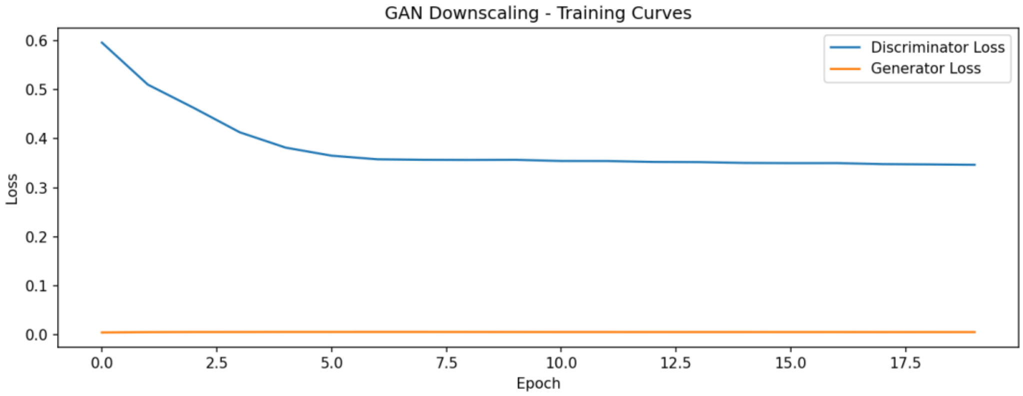

Fig. 9. GAN loss curve

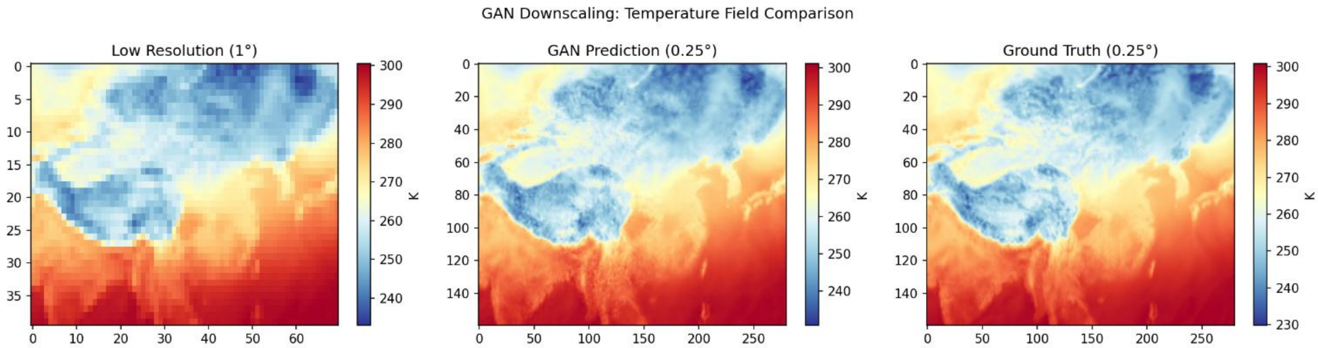

Fig. 10. GAN visual comparison

5) ***Diffusion Model Characteristics***

The diffusion model differs fundamentally from the other models in that it is generative rather than deterministic. Rather than producing a single prediction, it can generate an ensemble of plausible HR realizations from the same LR input by sampling the denoising chain multiple times. The standard deviation across these samples at each grid point provides a spatial map of prediction uncertainty, which is a valuable quantity for operational meteorological applications.

The noise prediction RMSE of 0.150 on the test set indicates that the UNet is reasonably effective at predicting the added noise given the LR condition. The training loss decreasing from 0.076 at epoch 1 to 0.021 at epoch 30 demonstrates consistent learning, though it had not converged by epoch 30. Full image quality evaluation was not performed, but qualitative examination of generated samples shows that the diffusion model produces spatially coherent temperature fields, with the spread across samples reflecting genuine uncertainty in the fine-scale structure.

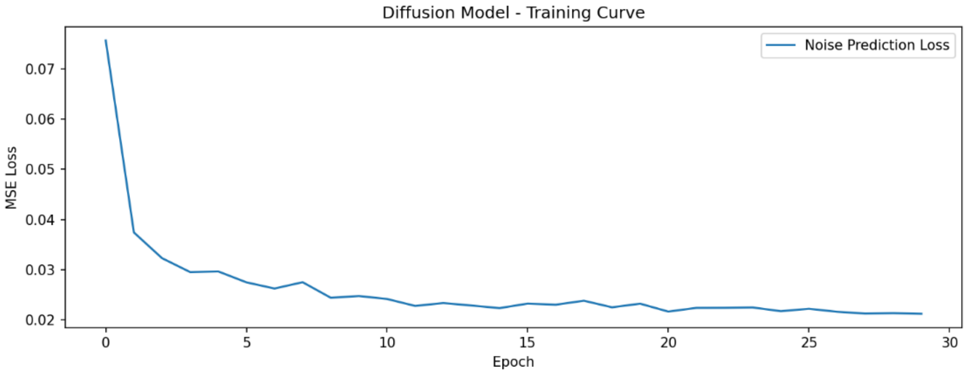

Fig. 11. Diffusion loss curve

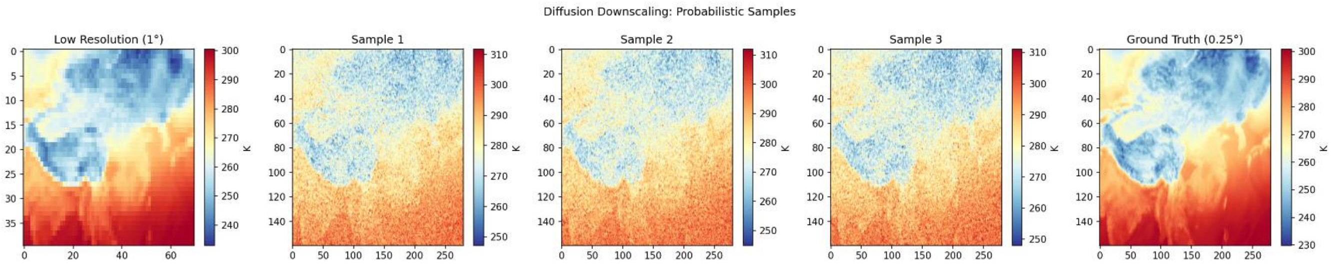

Fig. 12. Diffusion probabilistic samples

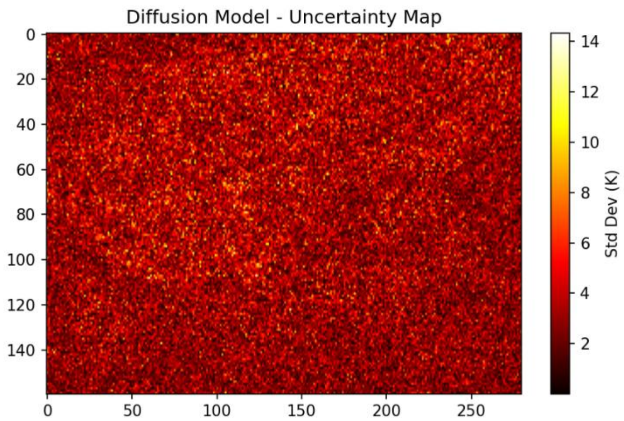

Fig. 13. Diffusion uncertainty map

IV. CONCLUSION

A. *Summary*

This experiment implemented, trained, and evaluated six deep learning models for ERA5 2m temperature downscaling from 1° to 0.25° resolution over the China region. The five baseline models span a broad range of architectural paradigms: convolutional (CNN), adversarial (GAN), sequential (LSTM), attention-based (Transformer), and generative (Diffusion). A novel Physics-Informed CNN was proposed and evaluated as the sixth model, combining multi-scale feature extraction, spatial attention, and physics-informed loss terms targeting spatial smoothness and energy conservation.

B. *Main Conclusions*

The following conclusions are drawn from the experimental results.

First, convolutional architectures with appropriate inductive biases are the most effective approach for meteorological downscaling at moderate dataset sizes (approximately 10,000 to 20,000 samples). Both the CNN and the proposed PICNN significantly outperform the Transformer and LSTM, which have far more parameters but less appropriate inductive biases.

Second, a controlled ablation study reveals that PICNN's improvement over the CNN baseline is only partially attributable to its physics-informed design. Approximately 65.5% of the improvement is explained by increased parameter count alone, independent of architecture. Among the three architectural components introduced, spatial attention provides the largest capacity-independent contribution, the physics-informed loss provides a smaller but consistent contribution, and the multi-scale feature extraction head shows no measurable benefit. This refines, rather than overturns, the conclusion that physics-informed design is valuable for meteorological downscaling: the evidence supports spatial attention and physics-informed loss terms specifically, rather than the PICNN architecture as a whole.

Third, model parameter count is not a reliable predictor of performance in data-limited meteorological settings. The 139M parameter Transformer performs worse than the 354K parameter CNN, and the 50M parameter LSTM performs worst of all. This challenges the assumption that larger models always perform better and highlights the importance of matching architectural design choices to the properties of the target domain.

Fourth, different models offer different value propositions beyond raw accuracy. The diffusion model provides uncertainty quantification that the other models cannot. The GAN offers the potential for perceptually sharper outputs with longer training. The LSTM captures temporal dependencies that purely spatial models ignore. Each has potential value in different operational contexts.

Fifth, training with reduced epochs due to hardware constraints affects all models but particularly affects large models like the Transformer and Diffusion, which converge more slowly. The reported results should be understood as lower bounds on potential performance rather than definitive comparisons.

C. Limitations

Several limitations of this work should be acknowledged.

The most significant limitation is the reduced training budget due to laptop hardware constraints. Models were trained for 20 to 30 epochs instead of the original 50 epochs, meaning none of the models were fully converged. The Transformer in particular showed no signs of converging by epoch 20, and its poor performance may improve substantially with more training.

The controlled ablation study reported in Section III.E.1 addresses the model-capacity confound identified in an earlier version of this analysis. However, the CNN baseline, the full PICNN, and the capacity-matched control (Variant A) were each trained with only a single random seed, so the specific finding that capacity explains approximately 65.5% of the improvement should be treated as indicative rather than statistically confirmed. Extending these three configurations to multiple seeds, as was done for the three component-ablated variants, would strengthen this estimate.

The evaluation is limited to a single variable (2m temperature) and a single domain (China region). Generalizability to other variables such as precipitation, which has more spatially discontinuous structure, or to other regions, has not been tested.
DataLoader workers were set to 0 due to Windows multiprocessing constraints, which limits data loading throughput and may have introduced data loading bottlenecks during training, particularly for larger models.

The diffusion model was not evaluated on image quality metrics due to inference time constraints, making direct comparison with other models incomplete.

D. Future Improvements

Based on the findings and limitations of this experiment, several directions for future improvement are identified.

Running all models to full convergence on a server-grade GPU would provide more reliable and fair comparisons. A model such as the Transformer that underperformed significantly with 20 epochs may become competitive with 100 or more epochs on a proper GPU cluster.

Repeating the ablation study with multiple random seeds for the CNN baseline, the full PICNN, and the capacity-matched control (Variant A) would strengthen the single-seed estimate that capacity explains approximately 65.5% of PICNN's improvement over the CNN baseline, complementing the three-seed results already obtained for the three component-ablated variants.

A ConvLSTM [8] baseline would be a more appropriate temporal model than the flat LSTM, as it preserves spatial structure throughout the recurrent processing and would likely perform significantly better.

A hybrid PICNN-Transformer model using windowed local attention (similar to Swin Transformer [11]) rather than global attention could combine the spatial inductive bias of CNNs with the long-range dependency modeling of Transformers, while remaining trainable on moderate-sized datasets.

Including additional atmospheric variables as auxiliary inputs, such as surface pressure, geopotential height at 500 hPa, and land-sea mask, would provide the model with more physical context and likely improve downscaling accuracy, particularly in coastal and mountainous regions.

Finally, extending the physics-informed loss to include additional constraints derived from the primitive equations of atmospheric motion, such as horizontal divergence consistency, would further align the training objective with known physical laws.

REFERENCE

1. H. Hersbach et al., "The ERA5 global reanalysis," Quarterly Journal of the Royal Meteorological Society, vol. 146, no. 730, pp. 1999-2049, 2020.

2. C. Dong, C. C. Loy, K. He, and X. Tang, "Image super-resolution using deep convolutional networks," IEEE Transactions on Pattern Analysis and Machine Intelligence, vol. 38, no. 2, pp. 295-307, 2016.

3. C. Ledig et al., "Photo-realistic single image super-resolution using a generative adversarial network," in Proc. IEEE Conference on Computer Vision and Pattern Recognition (CVPR), 2017, pp. 4681-4690.

4. P. Isola, J.-Y. Zhu, T. Zhou, and A. A. Efros, "Image-to-image translation with conditional adversarial networks," in Proc. IEEE Conference on Computer Vision and Pattern Recognition (CVPR), 2017, pp. 1125-1134.

5. Dosovitskiy et al., "An image is worth 16x16 words: Transformers for image recognition at scale," in Proc. International Conference on Learning Representations (ICLR), 2021.

6. J. Ho, A. Jain, and P. Abbeel, "Denoising diffusion probabilistic models," Advances in Neural Information Processing Systems, vol. 33, pp. 6840-6851, 2020.

7. S. Woo, J. Park, J.-Y. Lee, and I. S. Kweon, "CBAM: Convolutional block attention module," in Proc. European Conference on Computer Vision (ECCV), 2018, pp. 3-19.

8. X. Shi, Z. Chen, H. Wang, D.-Y. Yeung, W.-K. Wong, and W.-C. Woo, "Convolutional LSTM network: A machine learning approach for precipitation nowcasting," Advances in Neural Information Processing Systems, vol. 28, pp. 802-810, 2015.

9. P. Kingma and J. Ba, "Adam: A method for stochastic optimization," in Proc. International Conference on Learning Representations (ICLR), 2015.

10. I. Loshchilov and F. Hutter, "Decoupled weight decay regularization," in Proc. International Conference on Learning Representations (ICLR), 2019.

11. Z. Liu et al., "Swin Transformer: Hierarchical vision transformer using shifted windows," in Proc. IEEE/CVF International Conference on Computer Vision (ICCV), 2021, pp. 10012-10022.

APPENDIX

A.1 Dataset Construction and Normalization

```
class ERA5DownscalingDataset(Dataset):  3 usages
    def __init__(
        self,
        split="train",
        data_dir=PROCESSED_DIR,
        mmap=True,
        max_samples=None,
        return_time=False,
        n_samples=None,
        **_legacy_kwargs,
    ):
        if split not in REQUIRED_SPLITS:
            raise ValueError(f"split 必须是 {REQUIRED_SPLITS} 之一, 当前: {split}")

        if n_samples is not None and max_samples is None:
            max_samples = n_samples
```

```python
    def __getitem__(self, idx):
        lr = torch.from_numpy(
            np.array(self.lr_data[idx], dtype=np.float32, copy=True)
        ).unsqueeze(0)
        hr = torch.from_numpy(
            np.array(self.hr_data[idx], dtype=np.float32, copy=True)
        ).unsqueeze(0)

        if self.return_time:
            return lr, hr, str(self.time[idx])
        return lr, hr
```

A.2 CNN Residual Block

```python
class ResidualBlock(nn.Module):  2 usages
    def __init__(self, channels):
        super(ResidualBlock, self).__init__()
        self.conv1 = nn.Conv2d(channels, channels,  kernel_size: 3, padding=1)
        self.bn1 = nn.BatchNorm2d(channels)
        self.relu = nn.ReLU(inplace=True)
        self.conv2 = nn.Conv2d(channels, channels,  kernel_size: 3, padding=1)
        self.bn2 = nn.BatchNorm2d(channels)

    def forward(self, x):
        residual = x
        out = self.relu(self.bn1(self.conv1(x)))
        out = self.bn2(self.conv2(out))
        return out + residual
```

A.3 PICNN Multi-Scale Feature Extraction Head

```python
class PhysicsInformedLoss(nn.Module):  1 usage
    def __init__(self, lambda_smooth=0.1, lambda_conservation=0.05):
        super().__init__()
        self.mse = nn.MSELoss()
        self.lambda_smooth = lambda_smooth
        self.lambda_conservation = lambda_conservation

        laplacian = torch.tensor(
             data: [[0,  1, 0],
             [1, -4, 1],
             [0,  1, 0]], dtype=torch.float32
        ).view(1, 1, 3, 3)
        self.register_buffer = None
        self.laplacian = laplacian

    def forward(self, pred, target, lr_input):
        min_h = min(pred.shape[2], target.shape[2])
        min_w = min(pred.shape[3], target.shape[3])
        pred_a   = pred[:, :, :min_h, :min_w]
        target_a = target[:, :, :min_h, :min_w]

        l_mse = self.mse(pred_a, target_a)

        lap_kernel = self.laplacian.to(pred.device)
        pred_lap   = nn.functional.conv2d(pred_a,   lap_kernel, padding=1)
        target_lap = nn.functional.conv2d(target_a, lap_kernel, padding=1)
        l_smooth = self.mse(pred_lap, target_lap)

        # Energy conservation: spatial mean of prediction should match LR input mean
        pred_mean = pred_a.mean(dim=[2, 3])
        lr_mean   = lr_input.mean(dim=[2, 3])
        l_conservation = self.mse(pred_mean, lr_mean)

        total = l_mse + self.lambda_smooth * l_smooth + self.lambda_conservation * l_conservation
        return total, l_mse, l_smooth, l_conservation
```

A.4 Spatial Attention Module

```
class SpatialAttention(nn.Module):  1 usage
    """
    空间注意力：让模型聚焦于气象场中变化剧烈的区域
    (山脉、海陆边界等局部特征丰富的地方)
    """
    def __init__(self, kernel_size=7):
        super().__init__()
        self.conv = nn.Conv2d( in_channels: 2,  out_channels: 1, kernel_size, padding=kernel_size // 2)
        self.sigmoid = nn.Sigmoid()

    def forward(self, x):
        avg_pool = torch.mean(x, dim=1, keepdim=True)
        max_pool, _ = torch.max(x, dim=1, keepdim=True)
        pooled = torch.cat( tensors: [avg_pool, max_pool], dim=1)
        return x * self.sigmoid(self.conv(pooled))
```

A.5 Physics-Informed Loss Function

```
class PhysicsInformedCNN(nn.Module):  1 usage
    """
    物理信息CNN降尺度模型

    架构:
      1. 双线性上采样 (与基线CNN相同)
      2. 多尺度特征提取头
      3. 带空间注意力的残差块堆叠
      4. 重建尾部

    物理约束在损失函数中施加 (见 PhysicsInformedLoss)
    """
    def __init__(self, scale_factor=4, num_residual_blocks=8):
        super().__init__()
        self.upsample = nn.Upsample(
            scale_factor=scale_factor, mode='bilinear', align_corners=True
        )
        # Multi-scale head instead of single 9x9 conv
        self.head = MultiScaleBlock( in_channels: 1,  out_channels: 64)

        # Residual blocks with spatial attention
        self.residual_blocks = nn.Sequential(
            *[ResidualBlockWithAttention(64) for _ in range(num_residual_blocks)]
        )

        self.tail = nn.Sequential(
            nn.Conv2d( in_channels: 64,  out_channels: 32,  kernel_size: 5, padding=2), nn.ReLU(inplace=True),
            nn.Conv2d( in_channels: 32,  out_channels: 1,  kernel_size: 5, padding=2)
        )

    def forward(self, x):
        x_up = self.upsample(x)
        feat = self.head(x_up)
        feat = self.residual_blocks(feat)
        return x_up + self.tail(feat)
```

A.6 DDPM Forward Process and Training Objective

```
class DDPM:  1 usage
    def __init__(self, model, num_timesteps=1000):
        self.model = model
        self.T = num_timesteps
        self.betas = torch.linspace( start: 1e-4,  end: 0.02, num_timesteps)
        self.alphas = 1.0 - self.betas
        self.alphas_cumprod = torch.cumprod(self.alphas, dim=0)
        self.alphas_cumprod_prev = torch.cat([torch.tensor([1.0]), self.alphas_cumprod[:-1]])
        self.sqrt_alphas_cumprod = torch.sqrt(self.alphas_cumprod)
        self.sqrt_one_minus_alphas_cumprod = torch.sqrt(1.0 - self.alphas_cumprod)

    def q_sample(self, x_0, t, noise=None):  2 usages (1 dynamic)
        if noise is None: noise = torch.randn_like(x_0)
        device = x_0.device
        sa = self.sqrt_alphas_cumprod.to(device)[t].view(-1, 1, 1, 1)
        sm = self.sqrt_one_minus_alphas_cumprod.to(device)[t].view(-1, 1, 1, 1)
        return sa * x_0 + sm * noise

    def p_losses(self, x_0, condition, t):  1 usage (1 dynamic)
        noise = torch.randn_like(x_0)
        x_noisy = self.q_sample(x_0, t, noise)
        pred_noise = self.model(x_noisy, t, condition)
        min_h = min(pred_noise.shape[2], noise.shape[2])
        min_w = min(pred_noise.shape[3], noise.shape[3])
        return nn.functional.mse_loss(pred_noise[:,:,:min_h,:min_w], noise[:,:,:min_h,:min_w])
```

A.7 Evaluation Utility

```
def evaluate_image_model(
    model: nn.Module,
    test_loader,
    metadata: dict,
    desc: str = "Eval",
    max_batches: int = 0,
) -> dict:
    device = next(model.parameters()).device
    model.eval()

    mean, std = _get_norm_params(metadata)

    all_pred_n, all_tgt_n = [], []

    bar = tqdm(test_loader, desc=desc, ncols=100)
    for i, (lr_b, hr_b) in enumerate(bar):
        if max_batches and i >= max_batches:
            break
        lr_b = lr_b.to(device)
        pred = model(lr_b).cpu()

        # Align spatial dims in case of rounding differences
        min_h = min(pred.shape[2], hr_b.shape[2])
        min_w = min(pred.shape[3], hr_b.shape[3])
        pred = pred[:, :, :min_h, :min_w].numpy()
        tgt  = hr_b[:, :, :min_h, :min_w].numpy()

        all_pred_n.append(pred[:, 0])   # drop channel dim -> (B, H, W)
        all_tgt_n.append(tgt[:, 0])

    all_pred_n = np.concatenate(all_pred_n, axis=0)
    all_tgt_n  = np.concatenate(all_tgt_n,  axis=0)

    all_pred_k = _denorm(all_pred_n, mean, std)
    all_tgt_k  = _denorm(all_tgt_n,  mean, std)
```

```
    metrics = {
        "RMSE_norm": _rmse(all_pred_n, all_tgt_n),
        "RMSE_K":    _rmse(all_pred_k, all_tgt_k),
        "MAE_K":     _mae(all_pred_k,  all_tgt_k),
        "PSNR":      _psnr(all_pred_k, all_tgt_k),
        "SSIM":      _ssim_batch(all_pred_k, all_tgt_k),
    }
    return metrics
```